Partial CO$_2$ Reduction in Amorphous Cylindrical Silica Nanopores Studied with Reactive Molecular Dynamics Simulations

Tran Thi Bao Le and Alberto Striolo*

Department of Chemical Engineering, University College London, London WC1E 6BT
United Kingdom

David R. Cole

School of Earth Sciences, Ohio State University, Columbus, Ohio 43210
*United States*

ABSTRACT

It is known that pore confinement affects structure and transport properties of fluids. It has also been shown that confinement can affect the equilibrium composition of a reactive system. Such effects could be related to the possible abiotic hydrocarbons synthesis in deep-sea hydrothermal vents, especially when the CO$_2$ methanation reaction occurs within nanopores. In an attempt to identify possible rate-limiting steps of such reaction, we report here molecular dynamics simulations conducted implementing the reactive ReaxFF force field. The reaction is considered within a cylindrical nano-pore carved out of amorphous silica. Within the constraints of our simulations, which were conducted for 5 ns, no CH$_4$ molecules were detected in the temperature range $400-1000$ K, suggesting that the silica pore hinders the complete CO$_2$ reduction. This is consistent with the fact that silica is not an effective catalyst for CO$_2$ methanation. Our simulations, in agreement with literature reports, suggest that the silica pore surface facilitates the partial reduction of CO$_2$ to CO, which, within the conditions of our study, is found to be a stable product within the silica nanopores simulated. Analysis of the reaction products suggests that, although C-C bonds did not form, fragments reminiscent of carboxylic acids and formate were observed. Because these compounds are part of the biological Krebs cycle, our results suggest that confinement could provide pre-biotic precursors of core metabolic pathways. Our results could be useful for further developing applications in which catalysts are designed to promote CO$_2$ activation, for example the one-step thermolysis of CO$_2$.

* Corresponding Author: a.striolo@ucl.ac.uk

1. INTRODUCTION

Besides dramatic influences on the structure of fluids,[1-5] their transport properties,[6-10] and mutual solubility,[11-17] nano-confinement has been shown to affect chemical equilibria. The effects of confinement on chemical reaction equilibria for model, reversible reactions in slit-shaped pores were first reported by Borowko et al.,[18-19] while Turner et al.[20-23] reported molecular-level simulation studies for realistic, reversible reactions in carbon micropores and carbon nanotubes. Santiso et al.[24] implemented plane wave pseudopotential density functional theory (DFT) to simulate the rotational isomerization of 1,3-butadiene and the unimolecular decomposition of formaldehyde in slit-shaped pores formed by two parallel graphene sheets. Their results showed that confinement affects the potential energy profile for the isomerization of 1,3-butadiene, whereas the proximity of the pore surface reduces somewhat the activation energy. Turner et al.[25] predicted the rate constant for the hydrogen iodide decomposition reaction [$2HI \rightarrow H_2 + I_2$] in slit-shaped carbon pores and in carbon nanotubes by combining the transition-state theory formalism with Reactive Monte Carlo (RxMC) simulations.[26-27] The results suggested that the reaction rate in (8,8) carbon nanotubes increased by a factor of 47 compared to that observed for bulk fluids at the same thermodynamic conditions. These results illustrate the large effects that confinement and fluid–wall intermolecular forces can exert on the rate of a chemical reaction and on the equilibrium composition of a reactive system.

Building on this literature, Peng et al.[28] simulated the ammonia synthesis reaction in MCM-41 and pillared clays. Hansen et al.[29] quantified the influence of silicalite-1 pores on the reaction equilibria of propene metathesis reactions. Lísal et al.[30] studied the NO dimerization reaction in carbon slit nanopores in equilibrium with a bulk reservoir. In general, it has been reported that reaction rates in confinement differ from those in bulk because the favourable wall-fluid interactions can increase the reactants density and enhance the formation of transition state complexes. Such effects depend on pore size, pore chemistry and pore morphology.[21] For example, Furmaniak et al.[31] showed that, within activated carbons, decreasing pore size may increase or decrease the reaction yield, depending on the relative adsorption energy of reactants and products. The computational studies just summarized focused on pore-size effects on the equilibrium conversion by employing the RxMC algorithm, widely used to simulate chemically reacting systems.[23] Our group also implemented this approach to quantify the effect of confinement on the equilibrium composition for the CO_2 methanation reaction:[32]

$$CO_2 + 4H_2 \leftrightarrow CH_4 + 2H_2O \tag{1}$$
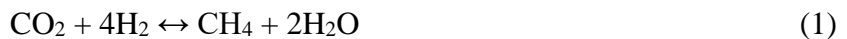
We compared the equilibrium composition of a reactive system composed of CO_2 and H_2 in confinement vs. that in the bulk phase at similar thermodynamics conditions. The study considered the possibility of abiotic hydrocarbons synthesis in sub-seafloor hydrothermal vents, and related discussions.[33-34] The abiotic synthesis of organic compounds involves the reduction of inorganic carbon sources such as CO_2 and CO by H_2, which could derive from either the oxidation of ferrous iron in basalt or the serpentinization of ultramafic minerals (e.g., olivine and pyroxene).[35-36] As an example of a recent contribution to this discussion, Menez et al.[37] reported evidence for the occurrence of aromatic amino acids formed abiotically at depth in oceanic crust. These authors suggest that the amino acids formation could have been

catalysed by an iron-rich saponite clay. It appears that iron catalysts play an important role. In fact, Muchowska et al.[38] recently showed that ferrous iron promotes a purely chemical reaction network by which CO_2 reduction yields many intermediates of the biological Krebs cycle. In our prior analysis, Reaction (1) was considered to occur in contact with slit-shaped pores carved out of β–cristobalite silica crystal. The reaction equilibrium composition was found to strongly depend on nanopore size and chemical features of the pore surface, and several scenarios were identified according to which the equilibrium CH_4 mole fraction in confinement exceeded that expected in bulk systems. The kinetics of the reaction was not considered.

Compared to the RxMC approach, reactive molecular dynamics (MD) simulations allow researchers to monitor the kinetics of a chemical reaction, and to identify the role of various catalysts. For example, reactive MD simulations conducted within the ReaxFF formalism were successfully employed to describe complex reactive chemical systems.[39-40] In the ReaxFF parameterisation, the bond order concept is implemented to determine inter-atomic interactions between all atoms within a chemical system. Therefore, when appropriately parameterised, ReaxFF provides an accurate description of the formation and dissociation of covalent bonds during dynamic simulations. ReaxFF captures short-lived molecular fragments and intermediates, which may not be considered in the RxMC approach, and could be difficult to be detected, even experimentally. ReaxFF parameters are obtained by fitting against training datasets containing quantum mechanical (QM) simulation results and experimental data. Accurate ReaxFF parameterisations have been applied to a wide range of reactive systems, including combustion processes,[41-44] the shock-induced chemistry of high-energy materials,[45-47] nanomaterials,[48-52] catalysts,[53-56] and also electrochemical phenomena.[57-59] Recently, we found that the ReaxFF parameterisation can predict structural and transport properties of non-reactive pure fluids (CH_4, CO_2, H_2O, and H_2).[60] However, our results showed that the agreement with both classical simulations and experiments depends strongly on the fluid considered and on the thermodynamics conditions simulated.

Better understanding the effect of confinement on both the composition and the kinetics of reactive systems could benefit many sectors, including the chemical industry, which makes large use of silica-based micro- and mesoporous materials as catalysts. Synthetic zeolites, for instance, are widely used for petroleum refining and other applications by the petrochemical industry.[61-62] As another example, mesoporous MCM-41 materials have recently been successfully applied as catalyst for the three-component Strecker reaction.[63]

Within this background, the main objective of the present study is to investigate, using the ReaxFF MD simulation approach, whether silica nanopores could promote the CO_2 methanation reaction (Reaction 1) at conditions consistent with those in our prior RxMC simulations.[32] This investigation is motivated by the observation that the equilibrium composition of systems that undergo Reaction (1) is expected to favour CH_4 production at low T, but due to the significant kinetic limitations of the eight-electron reduction of CO_2 to CH_4,[64] active catalysts are required for conducting such reaction industrially at acceptable rates and yields. A series of catalysts based on group VIII metals such as Ru,[65] Ni,[66-67] Pd[68] and Co[69] supported on porous materials such as TiO_2, Al_2O_3, CeO_2, MgO and zeolite have been tested and applied for CO_2 methanation.[70-73] None of these catalysts, nor iron-rich saponite clays are

directly considered in the present manuscript. It should also be noted that the time scales that can be investigated using the ReaxFF formalism are extremely short compared to typical experimental setups, and especially so when compared to chemical transformations that might occur in the sub-surface.

The rest of the manuscript is organized as follows: In Section 2, we first outline the ReaxFF formalism and then describe the simulation methodology implemented, including details on the solid support used to conduct the simulations. In Section 3, we present the results, starting from the expected equilibrium conversion for the CO_2 methanation (Reaction 1) based on thermodynamics calculations, followed by a detailed discussion of the reactive MD simulation results, first in the bulk and then in the amorphous silica nanopores. A discussion follows, in which we relate the present results to our prior RxMC calculations. Finally, in Section 4 we summarize our main conclusions.

2. COMPUTATIONAL DETAILS

2.1 Reactive Force Field Parameterisation – ReaxFF

ReaxFF is an empirical force field based on a chemical bond order/bond length relationship that allows bonds to dynamically dissociate and form. In the ReaxFF formalism, the instantaneous bond order, which is calculated and updated at every iteration from interatomic distances, is used to define all the connectivity-dependent interactions (e.g., valence and torsion-angles). The energies and forces associated with all bonded interactions disappear once the bonds dissociate. Non-bonded interactions (van der Waals and Coulomb) between all atom pairs are calculated from distance-corrected Morse and Coulomb potentials and are shielded at short distances to prevent excessive repulsions. In ReaxFF, the polarization of charges within molecules are obtained from the Electronegativity Equalization Method (EEM),[74] which is a geometry-dependent charge calculation approach. The general expression for the energy of the system, E_{system}, is given by

$$E_{system} = E_{bond} + E_{val} + E_{tors} + E_{over} + E_{under} + E_{lp} + E_{vdwaals} + E_{coulomb} \qquad (2)$$

The partial contributions to the total energy include bond energy (E_{bond}), valence angle energy (three body) (E_{val}), torsion angle energy (four body) (E_{tors}), over-coordination energy penalty (E_{over}), under-coordination stability (E_{under}), lone-pair energy (E_{lp}), non-bonded van der Waals ($E_{vdwaals}$) and Coulomb ($E_{coulomb}$) interactions, respectively.

We have chosen a recently published ReaxFF potential, which was developed for the Si/C/H/O system involved in the oxidation of SiC.[75] This parameter set is the combination of existing ReaxFF descriptions for hydrocarbons[76] and silicon/silicon oxides.[77-78] The set of ReaxFF parameters for C/H/O and Si/O/H materials to the silicon carbide materials were extracted from previously used Si/C, Si/O, Si/Si and Si/H quantum data for silicon,[79] silicon oxide,[77] and polydimethylsiloxide ReaxFF applications.[80] Details on the training of these data sets are provided by Newsome and co-workers.[75] It has been reported that the chosen Si/C/H/O

parameters are capable of describing reactions among hydrocarbons, as well as their reactions with silicon carbide, silicon oxides, diamond, and graphite materials.[75]

2.2 Simulation Methodology

All of the molecular dynamics (MD) simulations reported here were conducted using the ReaxFF reax/c code as implemented in the Large-scale Atomic/Molecular Massively Parallel Simulator (LAMMPS) package, version 20180818.[81-82]

The system was simulated as confined within a realistic cylindrical pore of diameter ~16 Å carved out of amorphous silica. A detailed description of the procedure implemented during the preparation of the cylindrical silica pore has been presented in a previous study,[83] in which we studied the transport properties of confined water-propane systems, using non-reactive force fields. In Figure 1A, we provide a schematic of the pore, which is found within a 57.28 Å x 57.28 Å x 57.28 Å simulation box with periodic boundary conditions along the 3 directions. The pore is parallel to the X axis of the simulation box. Because of periodic boundary conditions, the pore is infinitely long along the X direction. The surface of the cylindrical pore was saturated with hydroxyl groups and hydrogen atoms, yielding a hydroxyl density of $3.8/nm^2$. This is consistent with experimental measurements on flat amorphous silica surfaces.[84] The atoms within the silica substrate were fixed throughout the simulations, except for those atoms at the pore surface in contact with the fluid molecules.

In all simulations, a feed gas composed of CO_2 and H_2 was inserted in the pore, and then ReaxFF simulations were conducted to determine changes in system composition as simulation time progressed. Experimental evidence demonstrates that H_2/CO_2 ratio should not be lower than 4 to obtain high CH_4 selectivity and avoid carbon deposition during methanation.[85] Therefore, in all cases considered here, the feed gas consists of CO_2 and H_2 with a molar ratio of $H_2/CO_2 = 4$. This highly reducing composition was previously used to study the effect of confinement on the equilibrium composition implementing the RxMC approach.[32] A snapshot for the initial configuration of a system containing 50 CO_2 and 200 H_2 molecules confined in the amorphous silica cylindrical pore is shown in Figure 1B. Increasing the density of the reactants within the pore is expected to favour CO_2 methanation, based on results from our prior RxMC approach, and also based on the Le Chatelier's principle.
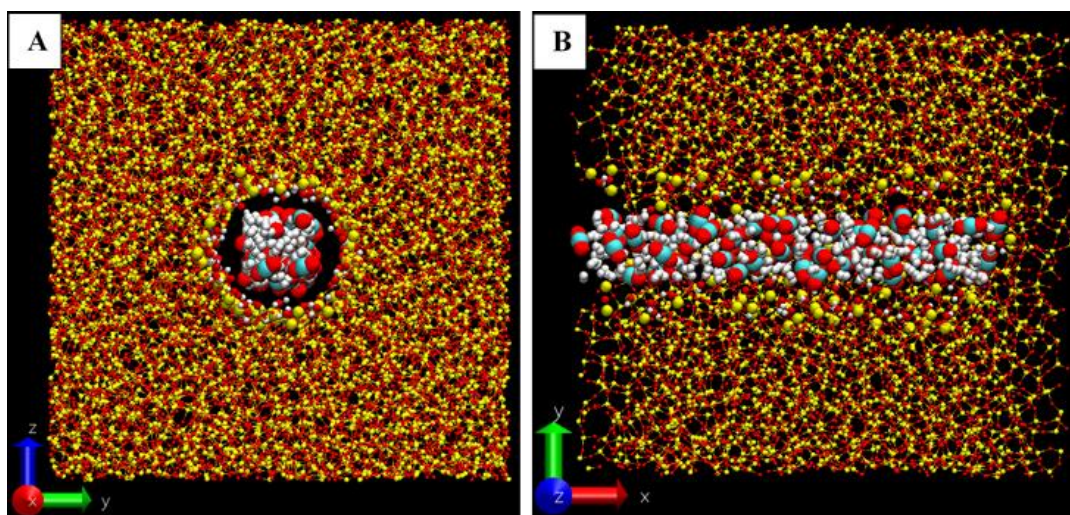
Figure 1. Snapshots of the initial system configuration from axial view (A) and side view (B). The yellow, red, cyan and white spheres represent Si, O, C and H atoms respectively.

The simulations were conducted within the constraints of constant number of atoms, constant volume and constant temperature – implementing the Nosé-Hoover thermostat with a temperature damping constant of 100 fs. The cutoff distance for electrostatic and van der Waals interactions is 10 Å. Although it is highly recommended to use tail corrections when simulating fluids in microporous materials,[86] the ReaxFF formalism as implemented in the present study was not trained to fit long-range London dispersion forces. In addition, Liu et al.[87] reported that the dispersion corrections have negligible effect on the description of chemical reactions.

The system temperature was set within the range from 400 K to 1000 K. The simulations were performed at 100 K temperature intervals, to investigate how the reaction product varies as a function of temperature. A time step of 0.25 fs was necessary to conserve the system energy at the chosen temperatures. At each temperature, we conducted 15 independent simulations to quantify the statistical reliability of the collected data. Each of the 15 simulations has a unique starting configuration and was initially equilibrated at low temperature and then heated to the target temperature.

The total simulation time for each system was determined by the extent of carbon dioxide reduction: simulations were terminated when no further change in system composition was observed within a simulated time of 5 ns. The kinetics of decomposition was studied by averaging the results from 15 simulations. Of the many key outcomes, one in particular quantified the dependency of the overall product distributions on the temperature of the system.
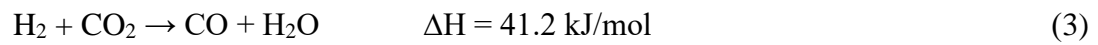
The bond, species and trajectory data extracted from the simulation output files were analyzed to track the number of molecular species generated during the simulations. A bond order cutoff of 0.3 was used for all bond types to identify the molecular species formed during the simulations. It has been shown that the bond order cutoff does not affect the final products obtained during a MD simulation, but only the formation of intermediates.[41] If the cutoff is too small, the simulation could identify too many bonds, affecting the computational efficiency;

on the other hand, too large a cutoff will yield fragmented molecules within the simulation. The 0.3 value has been widely used in the literature, yielding reliable results.[43, 88-89]

3. RESULTS AND DISCUSSION

3.1 Thermodynamic Analysis – Bulk System

The methanation of CO_2 as represented by Reaction 1 is a reversible and strongly exothermic reaction ($\Delta H = -165$ kJ/mol), which is favoured at low temperature, high pressure and high hydrogen fugacity.[90] The CO_2 methanation is the combination of the endothermic reversed water gas shift reaction (Reaction 3) and of the exothermic CO methanation (Reaction 4),[91] which are explicitly described as:

$$H_2 + CO_2 \rightarrow CO + H_2O \qquad \Delta H = 41.2 \text{ kJ/mol} \tag{3}$$

$$3H_2 + CO \rightarrow CH_4 + H_2O \qquad \Delta H = -206.1 \text{ kJ/mol} \tag{4}$$

The thermodynamic equilibrium for the three reactions (1), (3), and (4), can be quantified via the calculation of the equilibrium constants (K) via the van't Hoff equation:[92]

$$\frac{d\ln K}{dT} = \frac{\Delta h^o_{rxn}}{RT^2} \tag{5}$$

The van't Hoff equation, shown in Eq. (5), uses as input data the standard enthalpy of reaction, Δh^o_{rxn}, for each of the molecular compounds, which is a function of temperature. Obtaining the thermodynamic parameters for the reacting components from the literature,[93] we calculated the equilibrium constants as a function of temperature. The results, shown in Figure 2, are consistent with those reported by Gao et al.[85] It should be noted that in our prior work we calculated equilibrium quotients from the RxMC simulation results, rather than equilibrium constants, because the reaction was occurring within narrow pores, which affects the equilibrium composition and not the equilibrium constant. The results in Figure 2 are consistent with those reported previously,[32] when Reaction (1) occurs in the bulk.
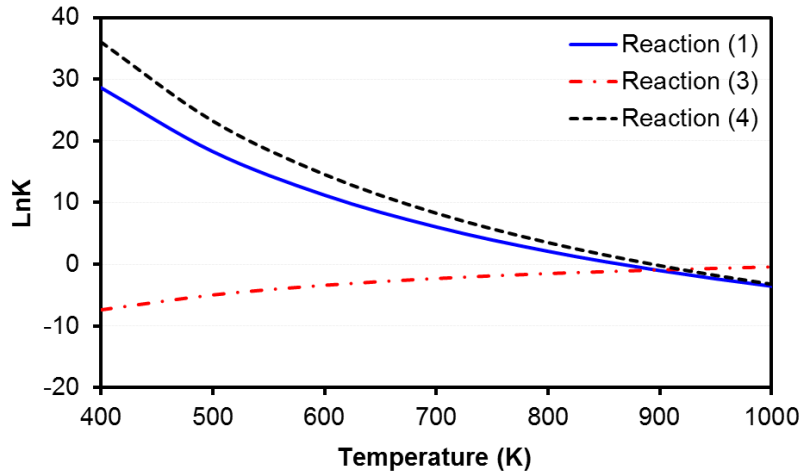
Figure 2. Equilibrium constants K calculated as a function of temperature for Reactions (1), (3), and (4), using Eq. (5) and standard enthalpy of reaction data from literature.

The results in Figure 2 show that both CO_2 and CO methanation reactions [Reactions (1) and (4), respectively], have high equilibrium constants in the temperature range 400–800 K, while the water gas shift Reaction (3) is characterized by lower K's at all temperatures. Gao et al.[85] obtained the equilibrium composition for CO_2 methanation implementing the total Gibbs free energy minimization method. We used the Aspen Plus software to calculate the system composition as a function of temperature when Reactions (1), (3), and (4) occur. In Figure 3 we report the equilibrium product mole fraction percent in the temperature range from 400 to 1000 K. The results in Figure 3 (c) demonstrate that at moderate temperatures (400–800 K) CO methanation is favoured in the bulk. At these conditions, the products mainly contain CH_4 and H_2O. When the temperature exceeds 800 K, the conversion of CO_2 into CH_4 is difficult to be achieved. In contrast, the conversion of CO_2 via Reaction (3) (the water gas shift reaction) increases with an increase in temperature (Fig. 3 b). This is due to the endothermic nature of Reaction (3), which is favoured at high temperature. Reactions (3) and (4) may simultaneously occur during CO_2 methanation, Reaction (1). Thus, irrespective of pressure, lower temperature favours CH_4 formation. However, it is well known that, due to kinetic barriers, the use of catalyst is essential to carry out the reaction at low temperatures.[64]
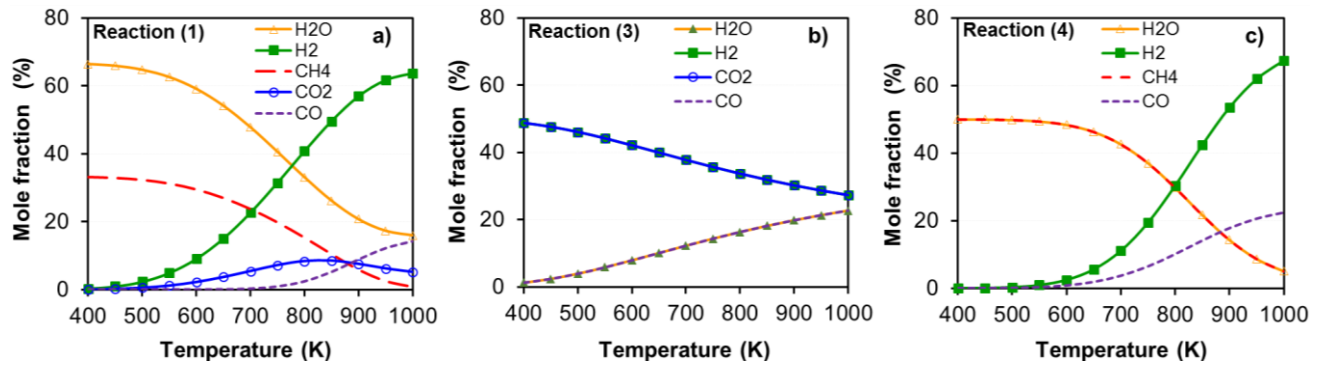

Figure 3. Equilibrium product composition of CO_2 methanation (a), water gas shift reaction (b) and CO methanation (c) calculated at 1 atm with a stoichiometric H_2/CO_2 molar ratio of 4.

3.2 ReaxFF Simulations of CO_2 Reduction in Bulk

In order to check whether the chosen ReaxFF parameters can adequately describe CO_2 reduction, and in particular, its transformation into CH_4, we tracked Reaction (1) in the bulk phase. To overcome the time scale limitations expected when implementing ReaxFF, we conducted this simulation at 2000 K. Although high temperature is unfavourable for CO_2 methanation, increasing temperature is necessary to speed up the reaction; this is a common practice to observe reactions in the nanosecond time scale in the absence of catalysts.[94-95] The reactants initial density considered in these simulations is consistent with those used for the simulations in the nanopores, discussed in Section 3.3, yielding a simulation box of dimensions 22 x 22 x 22 Å^3. Periodic boundary conditions were implemented in all directions. The initial configuration contained 50 CO_2 and 200 H_2 molecules. The same methodology was implemented to conduct ReaxFF simulations in bulk (this Section) and within the nanopore (Section 3.3).
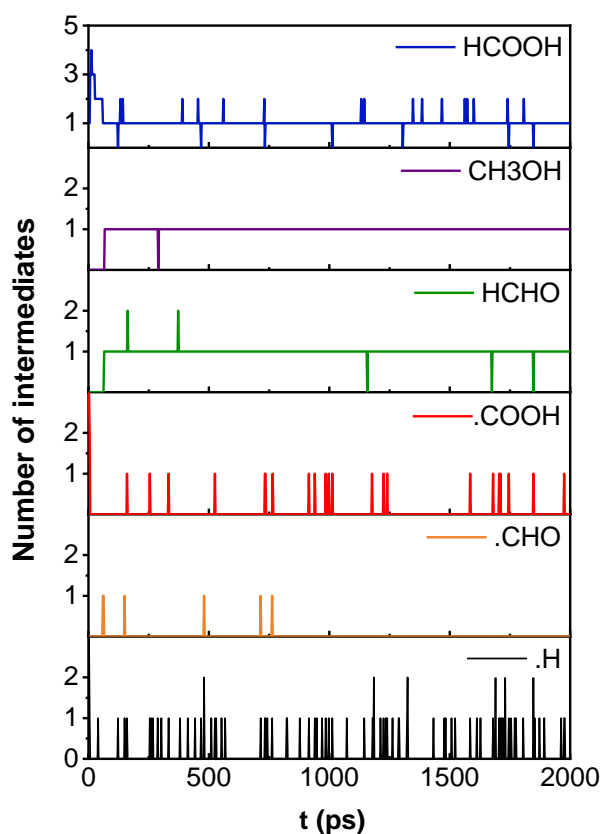

Figure 4. Main intermediates observed during the first 2 ns of partial CO_2 reduction [Reaction (1)] conducted in the bulk phase at 2000 K. The results shown here are from a single simulation, while the data shown later for the overall composition are the averages from 15 simulations.

The system composition as a function of simulation time is shown in Figure 4. Analysing the results, we observed some intermediates present for relatively long times: 1 CH_3OH and 1–2 HCHO and CH_2O_2 molecules were found during the first 2 ns of the simulations. These compounds remained in the simulated bulk systems at steady states. It should be noted that CH_2O_2 and HCHO play a key role in processes such as the oxidation of organic molecules and combustion,[96-97] and CH_3OH is one of the important intermediates observed during the conversion of $\cdot CH_3$ radicals into HCHO molecules in the gas explosion process.[98]

The distribution of major reactants and products as a function of simulation time for the bulk Reaction (1) is reported in Figure 5. Although some of these compounds are not experimentally stable at 2000 K; the simulation results suggest that, at the conditions considered, the water-gas shift reaction (Reaction 3) dominates, because of the high temperature (2000 K). Differences between the results of Figure 5 and those predicted by Figure 3 are largely ascribed to the fact that for the thermodynamics calculations of Figure 3, oxygen-containing compounds such as formaldehyde, methanol, formic acid and others were not considered. The product composition shown in Figure 5 reflects high CO content, which is also consistent with the thermodynamics calculations shown in Figure 3. In our simulations, the number of both CO and CH_4 molecules increased as the reaction proceeded. However, the amount of CO was found to be much larger than that of CH_4. After ~ 71 ns of simulations, our results show that the amount of CH_4 reached a constant value, and steady states were achieved.
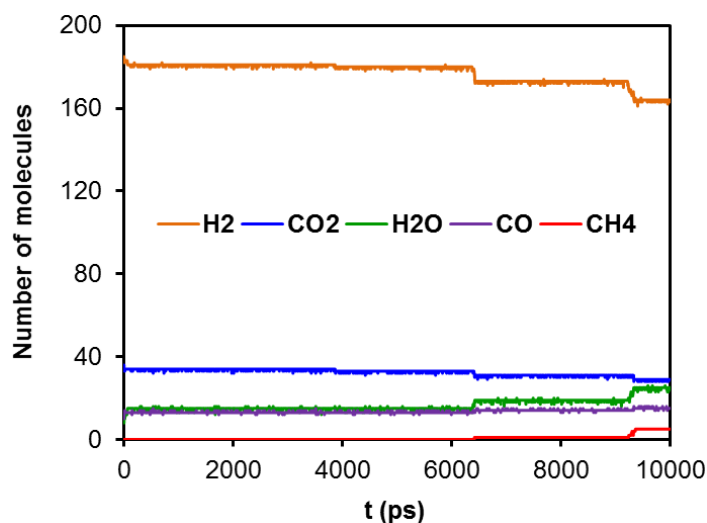

Figure 5. Evolution over the time of major reactants and products in the bulk reactive system simulated at 2000 K. Note that these results are from a single simulation.

In Figure 6, we summarize the compositions of the bulk system, as predicted by the ReaxFF MD simulations conducted at 2000 K. Besides CH_4 and CO, which are the main products, some by-products are present, albeit in small amounts. It should be noted that the results in Figure 6 reflect the averages obtained from 15 independent bulk simulations (each of up to 100 ns). Each simulation was interrupted when the system composition did not change for at least 60 ns. Once stable system compositions were achieved, each simulation was continued for an

additional 10 – 20 ns to further ensure that the final composition would not change. The results, shown in Figure 6, yield an average CH_4 mole fraction of ~ 2%, which is larger than that of less than 0.01% predicted from the total Gibbs free energy minimization method shown in Fig. 3 (a). These results confirm that the ReaxFF parameterisation is able to describe CO_2 reduction. The deviation in system composition predicted by the ReaxFF approach compared to the thermodynamic analysis is possibly due to the fact that the ReaxFF allows the formation of several intermediates, which are not considered in the thermodynamic analysis of Section 3.1.
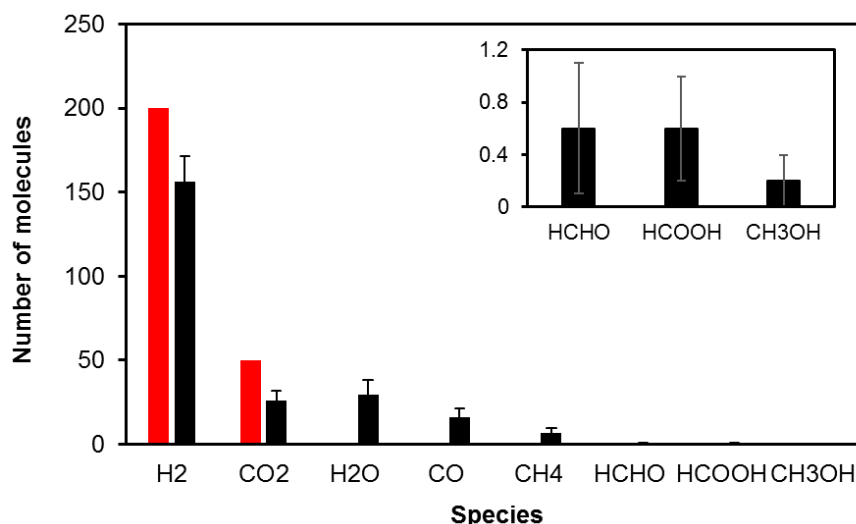

Figure 6. System composition obtained at 2000 K from the CO_2 reduction initiated from a system containing 50 CO_2 and 200 H_2 molecules in the bulk phase. The results are ensemble averages collected from 15 independent simulations. The initial composition is represented in red. In the inset we expand the results for HCHO, HCOOH and CH_3OH.

3.3 ReaxFF Simulations of Partial CO_2 Reduction in Nanopores

In Figure 7, we report typical simulation output data as observed within a silica pore, wherein the evolution of the system composition is plotted as a function of the simulation time. This simulation was conducted at 700 K, because thermodynamic analysis displayed in Figure 3 indicated at this temperature methane production is thermodynamically favoured, and this temperature may be high enough to overcome possible kinetic barriers. However, as shown in Figure 7, no CH_4 was found within the time scale of the simulations. The number of CO_2 molecules decreased gradually from 50 to 38, while 11 CO molecules were formed within the first 5 ps of the simulation. The numbers of CO_2 and CO molecules in the system remained almost constant after 5 ps. Meanwhile, the number of H_2 molecules decreased steadily; 51 H_2 molecules were consumed when the reaction proceeded to 5 ns. The number of H_2O molecules produced during the reaction increased slightly; 14 H_2O molecules were obtained at the end of the 5 ns simulation. The results suggest that, within the silica nanopore, CO_2 is reduced to CO quickly at the beginning of the simulation, but then the reaction ceases, at least within the time frame accessed by our simulations, while H_2 continues to be consumed, in part to yield H_2O.
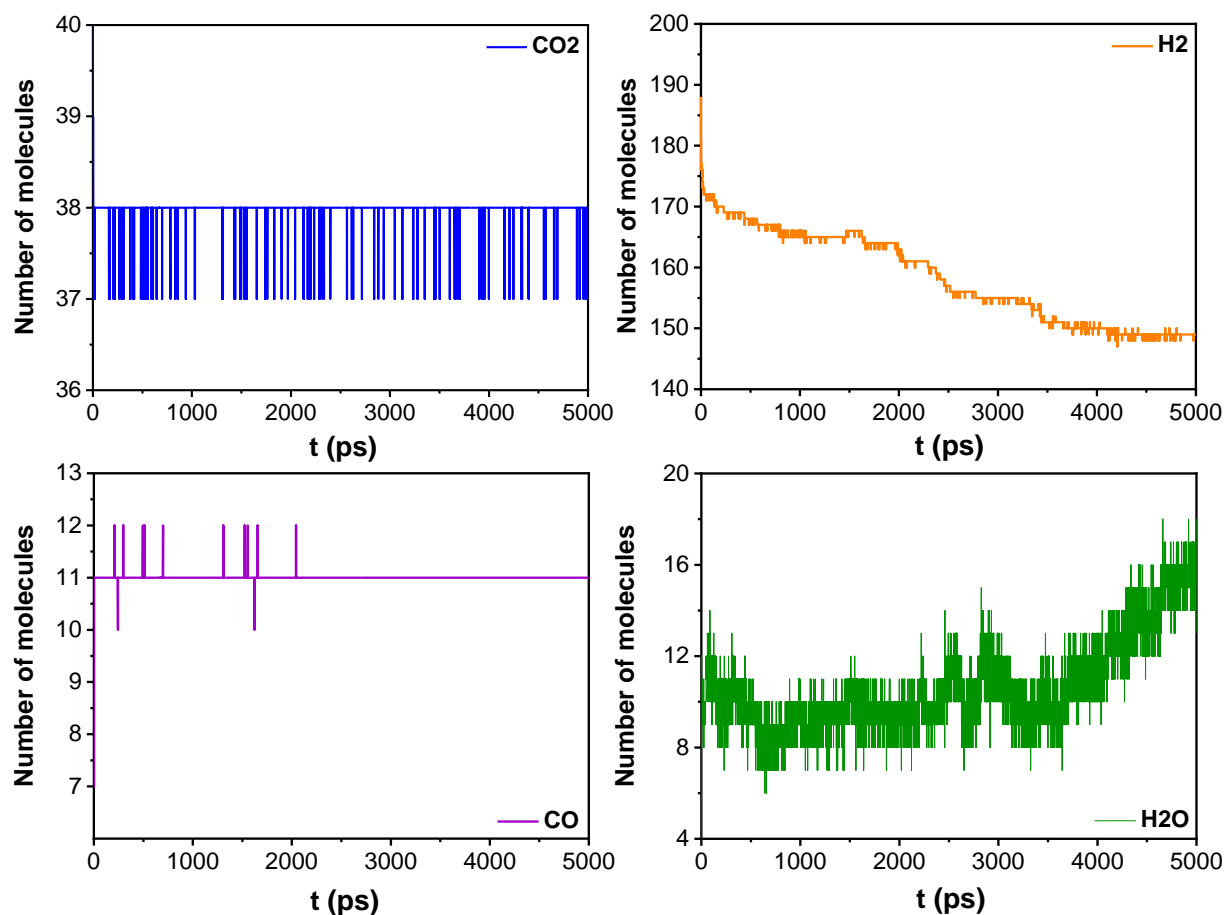
Figure 7. Representative results for the changes in system composition as a function of simulation time during the ReaxFF MD simulations of the partial CO_2 reduction within silica nanopores. Only CO, CO_2, H_2, and H_2O are monitored in this figure. The simulation was conducted at 700 K within an amorphous cylindrical silica nanopore. The figure only shows results from one simulation, not the average of the 15 simulations conducted at 700 K, which are reported below.
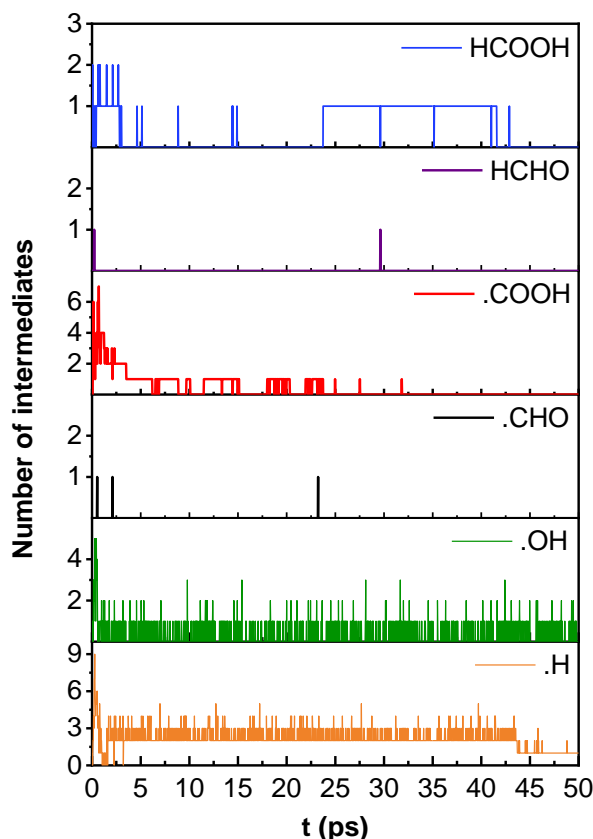
Figure 8. Intermediates system composition as a function of simulation time within the first 50 ps of the simulation conducted at 700 K in a silica nanopore. Note that these results are from a single simulation.

In the initial stages of the simulations, we observed numerous intermediate species, including ·COOH, ·CHO, HCHO and CH_2O_2, which were present for short simulation times and only in small quantities (see Figure 8). In light of the recent report by Muchowska et al.,[38] we find it interesting that some of the intermediates shown in Figure 8 represent fragments of carboxylic acids, formate, and other metabolic precursors. It is possible that, in the presence of iron-based catalysts, the spontaneous reduction of CO_2 within the system considered here could yield pre-biotic precursors of core metabolic pathways. However, in our system no catalyst was present. Returning to the analysis of the system composition as a function of simulation time (Figure 8), we note that ·OH and ·H free radicals were observed throughout the simulations. The decomposition of CO_2 into CO generated short-lived ·O radicals, which combined with ·H radicals to form ·OH radicals. The dissociation of H_2 produced ·H radicals. Free ·OH and ·H radicals were also generated from the dissociation of silanol groups on the silica surface. The amount of ·OH radicals remained low (1 or 2 after 5 ps), but 20 ·H radicals were observed when the simulation was interrupted at 5 ns (no additional CO production was observed when slightly longer simulations, up to 7 ns, were conducted). During the course of our simulations, it was observed that most of the ·H free radicals reacted with ·OH to yield H_2O molecules.

We conducted similar simulations within a range of temperature from 400 to 1000K. At each temperature, the system composition was found to become stable after a transient period. In Figure 9, we report the composition of the reactive systems once the composition did not change further (within the simulation times allowed by the ReaxFF simulations within the computing resources available to us). In none of the simulations conducted, which initially contained 50 CO_2 and 200 H_2 molecules, methane generation was observed. The reactive systems were found to contain CO, H_2O, and an excess amount of CO_2 and H_2. Our results show that as the temperature increases from 400 to 600 K, the amount of unreacted CO_2 increased, while the amount of CO and H_2O present within the system decreased. The amount of unreacted H_2 did not change significantly in this temperature range, which supports the hypothesis that the CO_2 methanation did not occur as the temperature fell below 600 K. When the systems were heated up to 700 K, the excess reactants amount decreased, while that of the main products increased. At higher temperatures, the quantities of excess CO_2 and CO produced no longer changed significantly, up to 1000 K, indicating that the increase in temperature did not promote the formation of CO. In contrast, the amount of H_2O increased constantly as temperature increased. An analysis on the system molecular composition based on the simulation results shown in Figure 9 suggests that partial CO_2 reduction to CO occurs at temperatures of 700 K and above, although increasing the temperature above 700 K does not seem to enhance strongly the extent of the reduction.

Our results, summarized in Figure 9, suggest that the silica substrate does not function as a catalyst for Reaction (1). At first, this result appears to be at odds with our prior findings, in which Le et al.,[32] using the RxMC approach, found that confinement can shift the equilibrium composition of Reaction (1) towards methane generation. The predicted shift in the equilibrium composition towards enhanced methane formation within silica nanopores was due to the fact that the hydrophilic pore surface effectively removed water, one of the products, from the reactive environment, and that confinement effectively enhanced the pressure of the reacting system. Based on Le Chatelier's principle, both these phenomena shift the equilibrium composition to higher CH_4 production. The RxMC approach did not consider the kinetics of the reaction, as only the equilibrium composition was sampled. The present study employs the ReaxFF formalism, which tracks the reaction kinetics, although reaching equilibrium might require prohibitive computing resources. The absence of CH_4 from the reaction products could simply be due to the fact that silica is not a catalyst for Reaction (1). Future efforts shall explore the evolution of CO_2 reduction within iron-rich saponite clays, which were considered essential for the abiotic production of aromatic amino acids in a recent experiment by Menez et al.[37]

To ensure that the ReaxFF MD simulations yield a structure of the confined fluid mixture similar to the one observed in our prior Monte Carlo simulations, in Figure 10 we report density profiles for H_2O, as well as other compounds, within the amorphous cylindrical silica pore. The density profile obtained for water (shown in the inset of Figure 10) is characterized by two pronounced peaks which are near to the pore surface, indicating the strong adsorption of water on the surface. This is consistent with our prior results, although water is present in small amounts in the systems considered here. The positions of CO_2 and H_2 density peaks are approximately identical, which is consistent with those reported in our previous Monte Carlo

simulations. While H_2 and CO occupy the entire pore volume yielding a more or less homogeneous distribution, CO_2 is found preferentially in proximity of the silica pore surface, where it can form hydrogen bonds with the –OH groups on the surface. It should be pointed out that the density profiles suggest that H_2 is somewhat depleted in the pore center, possibly because its preferential adsorption on the pore surface. It is discussed later that this partition could directly affect the reaction mechanism.
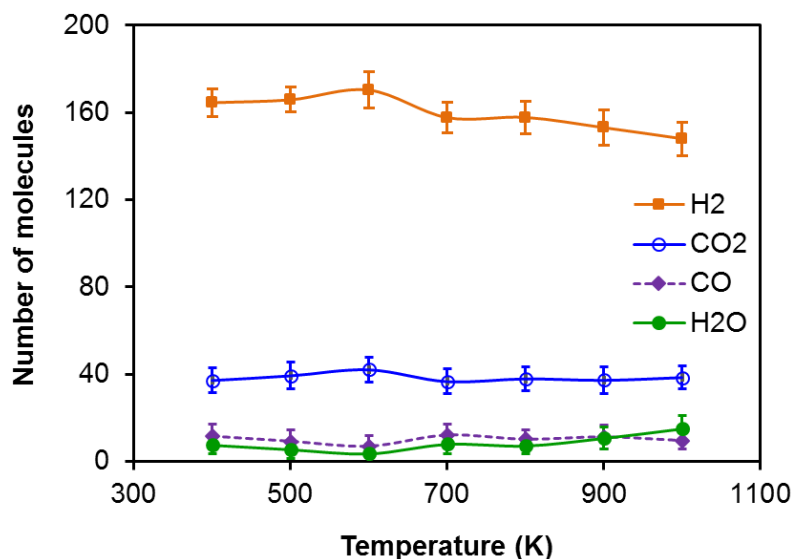

Figure 9. Molar composition at steady states as obtained from the MD simulation of the hydrogenation of CO_2 implementing the ReaxFF approach for systems confined in the cylindrical silica pores shown in Figure 1. In all cases, the initial system contains 50 CO_2 and 200 H_2 molecules. The simulations are conducted for 5 ns. System compositions during the last 1 ns of the simulations are used as ensemble averages. Error bars (vertical lines) are estimated as one standard deviation from the average.

Returning to Figure 9, the results, affected by rather large uncertainty, show very weak dependence on temperature. Perhaps, the results suggest that CO_2 methanation did not occur within the silica nanopores when temperature was below 700 K, within the constraints of our simulations. This could be due to several factors. It could be that computational limitations prevent us from achieving equilibrium. It could also be that, at the conditions considered, the reversed water-gas shift Reaction (3) dominates. Increasing temperature does not affect this scenario because, as documented from Figure 2, Reaction (3) is characterized by lower K within the entire temperature range considered. The results in Figure 3 suggest that low temperature promotes CO_2 methanation, but, as is the case for industrial processes, it could be that such reaction is kinetically limited, and therefore no CH_4 generation was found in our simulations.
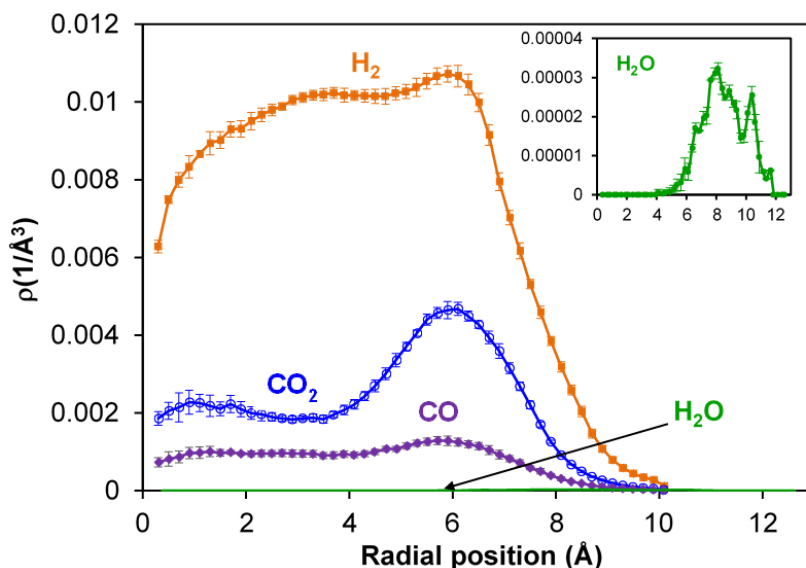
Figure 10. Density profiles of CO_2, H_2, CO and H_2O during the last 1 ns of the CO_2 methanation reaction at 700 K. In this graph, radial position =0 corresponds to the center of the cylindrical pore. We report the atomic density profiles of molecular center of mass. Note that the molecules found at radial distances larger than 0.8 nm correspond to a few molecules that penetrated the amorphous material, sometimes in correspondence of enhanced surface roughness. Error bars are estimated as one standard deviation from the average.

Comparing the composition of the reactive system in the bulk at 2000 K (Figures 4, 5, and 6) vs. that observed within the silica pores (Figures 8 and 9), it is noted that key intermediates such as ·COOH, ·CHO, HCHO and CH_2O_2 are present throughout the process in the bulk, but are only present for a short transient time (~ 50 ps) when the reaction occurs in the silica pore. Therefore, the lack of CH_4 formation in confinement could be due to the inability of these intermediates to persist in proximity of the silica substrate.

Although the results in Figure 9 do not reveal the formation of CH_4, they show that CO_2 is partially reduced to CO within the nanopores during our simulations. This observation could be of practical interest. It is in fact known that surface oxygen vacancies are the dominant defect in crystalline and amorphous silica.[99] Surface oxygen vacancies promote adsorption and activation of CO_2, even in the absence of H_2.[100-101] For example, Jiang et al.[102] recently reported on the one-step thermolysis of CO_2 in the presence of metal oxide surfaces. They found that porous silica oxide materials with large specific surface areas (e.g., SBA-15, MCM-41, commercial SiO_2) enhance the rate of CO_2 splitting into CO and O_2. It was suggested that the surface oxygen vacancies in the redox metal could act as catalyst for this reaction.

To test whether similar phenomena could occur for the system considered here, we conducted an additional test in which we removed H_2 from the reactive system within the amorphous silica pores and ran ReaxFF simulations at the conditions described in Figure 9. We conducted these simulations in the temperature range 400-1000 K. A typical evolution of the system composition is reported in Figure 11, which refers to a simulation conducted at 700 K. At the

beginning of the simulation ($0 - 3$ ps), we observed some free radicals ($\cdot$O, $\cdot$H, $\cdot$OH and $\cdot$COOH) released in relatively large amounts. However, after 100 ps the quantities of $\cdot$O, $\cdot$H and $\cdot$OH no longer increased and no $\cdot$COOH free radicals were observed. We observed that for the systems considered, the formation of CO was associated with the production of H_2O molecules, albeit in small amounts, rather than O_2. The amount of CO obtained at the end of the simulations as a function of temperature is shown in Figure 12. The results demonstrate that an appreciable amount of CO molecules formed even at much lower temperatures than those considered by Jiang et al.[102] for the direct thermolysis of CO_2, in the absence of H_2. The hydrogen atoms required for the formation of H_2O were obtained from the silica surface.

To visually quantify the effect of temperature on the results, we plot in Figure 12 the amount of CO obtained at simulation completion as a function of temperature. The results indicate that CO production increases as the temperature increases within the SiO_2 nanopores of Figure 1. It is interesting to note that the quantity of CO obtained from the direct partial reduction of CO_2 in confinement appears to be much larger than that obtained from the CO_2 methanation (i.e., see Figure 9). Therefore, our results seem to suggest that the presence of hydrogen in large amounts could hinder CO formation within silica nanopores. This could be a consequence of the fact that increasing the density within the silica nanopore by the addition of H_2 reduces the collision rate of CO_2 against the silica surface (i.e., see density profiles in Figure 10). This observation is clearly at odds with the general recommendation to maintain the H_2/CO_2 ratio larger than 4 to achieve high CH_4 selectivity in CO_2 methanation reaction and avoid carbon deposition during methanation,[85] although it should be pointed out that those recommendations are valid in the presence of catalytic materials.

While it is not surprising that amorphous silica is not an effective catalyst for CO_2 reduction, analysis of the simulation results can reveal the mechanisms responsible for this observation. We refer to the density profiles of H_2 and CO_2 within the silica nanopores tracked during the 700 K simulations, which are shown in Figure 10. It can be seen that although CO_2 and H_2 molecules distribute along the radial direction, perpendicular to the pore wall, the quantity of H_2 molecules residing close to the surface is much larger than that of CO_2, which supports the hypothesis that H_2 prevents CO_2 collisions with the surface.
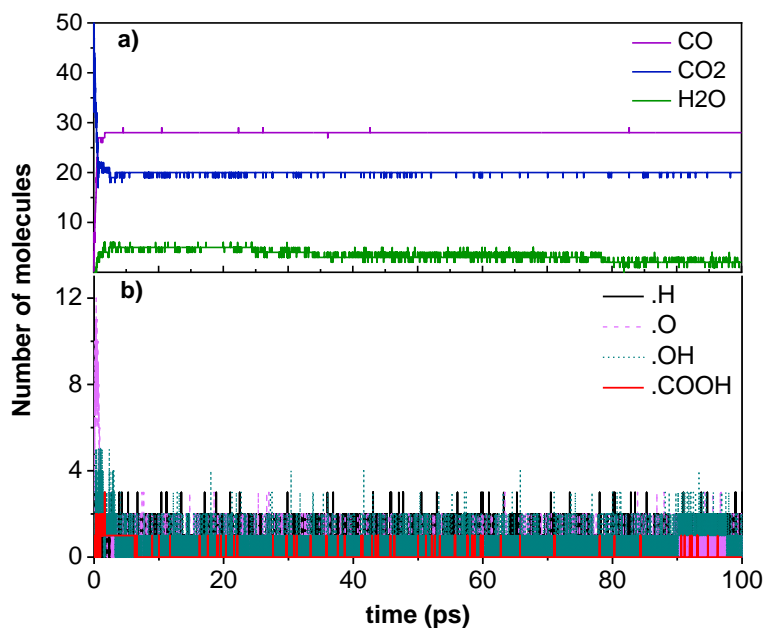
Figure 11. Evolution over time of a) reactants and products and b) major intermediates for the partial reduction of CO_2 within cylindrical silica pores at 700 K.
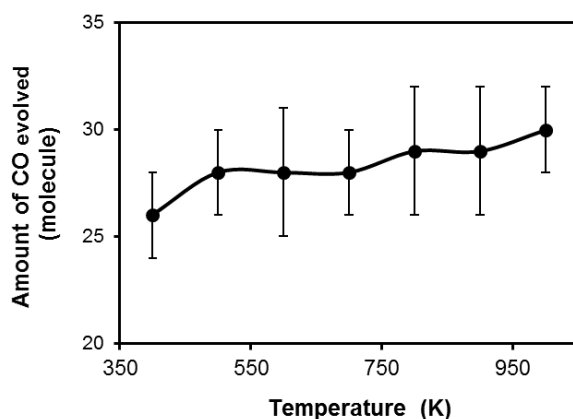

Figure 12. Amount of CO obtained from the partial reduction of CO_2 within cylindrical silica pores. In all cases, the initial system contains 50 CO_2 molecules, and the simulations are conducted for 5 ns. System compositions during the last 1 ns of the simulations are used as ensemble averages. Error bars are estimated as one standard deviation from the average.

To gain mechanistic insights into CO_2 dissociation, as described by the ReaxFF MD simulations, we performed a bond order analysis.[103] The CO_2 molecules collide with the defective silica surface, which initiates decomposition of CO_2 to CO molecules and generate ·O free radicals. When only CO_2 molecules are present within the pore, their collision with the surface yields the dissociation of silanol groups from silica, generating ·H and ·OH free radicals. This creates the possibility for ·H radicals to combine with ·OH radicals, yielding H_2O. Both CO_2 splitting and CO oxidation (CO + ½ O_2 = CO_2) occur simultaneously. In addition, CO molecules can contact ·OH radicals to yield short-lived ·COOH species, which are detected in the initial stages of our simulations. This radical is very active and has been considered a

precursor for CO formation.[104] As mentioned earlier, silica provides oxygen vacancies which promote the CO_2 splitting into CO. It is possible that CO is not reactive enough under our simulation conditions to react with H_2 and yield CH_4.

4. CONCLUSIONS

It is known that confinement has an effect on many physical properties of fluids. In particular, our group has considered the possibility that confinement affects the equilibrium distribution of oxidized vs. reduced carbon.[105] In our prior contribution,[32] we employed the RxMC approach to quantify the equilibrium composition of a system in which CO_2 came in contact with large amounts of H_2 in the presence of narrow hydrophilic silica-based pores. The results showed that, for the most part because the pore surface effectively removed H_2O from the products, the system composition was biased towards producing more CH_4 than it would have been expected based on thermodynamics calculations conducted in the bulk. This paper probes the specific question – can the CO_2 reduction be driven entirely inside cylindrical amorphous silica nanopores? The results confirm that amorphous silica is not a catalyst for the reaction, as is widely known. A better catalytic substrate choice would be TiO_2, Fe_3O_4, a FeNi bimetallic, or an Mg, Fe olivine with some trace or minor Cr, Ni or Co at the pore surface. All of these phases exist in oceanic crustal rocks. Future studies should consider these materials, in an attempt to connect simulation studies such as this one with experimental observations for methane seeps in marine hydrothermal vents,[33-34] aromatic amino acids formed abiotically at depth,[37] and intermediates of the biological Krebs cycle observed during CO_2 reduction.[38]

In summary, ReaxFF molecular dynamics simulations were employed to assess the potential partial reduction of CO_2 within cylindrical pores carved out of amorphous silica. Simulating the CO_2 methanation in the bulk phase at 2000 K shows the formation of CH_4 molecules, with a product composition generally consistent with thermodynamics calculations. ReaxFF MD simulations of pure CO_2 within the silica pores showed evidence of its partial reduction at moderate temperatures, yielding large amounts of CO. Analysis of these simulations showed that CO is produced directly from the collision of CO_2 with silica surface, on which defective sites could enhance CO_2 activation. When the ReaxFF MD simulations were conducted for CO_2 in presence of excess H_2 within the silica nanopores, partial reduction was observed, but no CH_4 was obtained at the conditions considered because the silica support reduces the concentration of some important intermediates, which seem to promote CO_2 reduction in the bulk. The results presented, and in particular the analysis of the reaction pathway, could be helpful for designing catalytic processes for the one-step thermolysis of CO_2. To be of relevance for quantifying the catalytic reduction of CO_2 in the presence of excess H_2, the study should be extended to materials containing appropriate catalysts, for example a Fe olivine with minor amounts of transition or noble metals at the pore surface.

Acknowledgments

References

1.   Porion, P.; Faugère, A. M.; Rollet, A.-L.; Dubois, E.; Marry, V.; Michot, L. J.; Delville, A. Influence of Strong Confinement on the Structure and Dynamics of Liquids: A Study of the Clay/Water Interface Exploiting ^{2}H NMR Spectroscopy and Spin-Locking Relaxometry. *J. Phys. Chem. C* **2018**, *122*, 16830-16841.

2.   Ho, T. A.; Argyris, D.; Cole, D. R.; Striolo, A. Aqueous NaCl and CsCl Solutions Confined in Crystalline Slit-Shaped Silica Nanopores of Varying Degree of Protonation. *Langmuir* **2012**, *28*, 1256-1266.

3.   Malani, A.; Ayappa, K. G. Relaxation and Jump Dynamics of Water at the Mica Interface. *J. Chem. Phys.* **2012**, *136*, 194701.

4.   Lee, S. S.; Fenter, P.; Park, C.; Sturchio, N. C.; Nagy, K. L. Hydrated Cation Speciation at the Muscovite (001)-Water Interface. *Langmuir* **2010**, *26*, 16647-16651.

5.   Rice, S. A. Structure in Confined Colloid Suspensions. *Chem. Phys. Lett.* **2009**, *479*, 1-13.

6.   Bui, T.; Phan, A.; Cole, D. R.; Striolo, A. Transport Mechanism of Guest Methane in Water-Filled Nanopores. *J. Phys. Chem. C* **2017**, *121*, 15675-15686.

7.   Franco, L. F. M.; Castier, M.; Economou, I. G. Anisotropic Parallel Self-Diffusion Coefficients near the Calcite Surface: A Molecular Dynamics Study. *J. Chem. Phys.* **2016**, *145*, 084702.

8.   Phan, A.; Cole, D. R.; Weiß, R. G.; Dzubiella, J.; Striolo, A. Confined Water Determines Transport Properties of Guest Molecules in Narrow Pores. *Acs Nano* **2016**, *10*, 7646-7656.

9.   Gautam, S.; Liu, T. T.; Rother, G.; Jalaivo, N.; Marmontov, E.; Welch, S.; Sheets, J.; Droege, M.; Cole, D. R. Dynamics of Propane in Nanoporous Silica Aerogel: A Quasielastic Neutron Scattering Study. *J. Phys. Chem. C* **2015**, *119*, 18188-18195.

10.   Chathoth, S. M.; He, L.; Mamontov, E.; Melnichenko, Y. B. Effect of Carbon Dioxide and Nitrogen on the Diffusivity of Methane Confined in Nano-Porous Carbon Aerogel. *Microporous Mesoporous Mater.* **2012**, *148*, 101-106.

11.   Badmos, S. B.; Striolo, A.; Cole, D. R. Aqueous Hydrogen Sulfide in Slit-Shaped Silica Nanopores: Confinement Effects on Solubility, Structural, and Dynamical Properties. *J. Phys. Chem. C* **2018**, *122*, 14744-14755.

12.   Gadikota, G.; Dazas, B.; Rother, G.; Cheshire, M. C.; Bourg, I. C. Hydrophobic Solvation of Gases (CO_2, CH_4, H_2, Noble Gases) in Clay Interlayer Nanopores. *J. Phys. Chem. C* **2017**, *121*, 26539-26550.

13.   Moučka, F.; Svoboda, M.; Lísal, M. Modelling Aqueous Solubility of Sodium Chloride in Clays at Thermodynamic Conditions of Hydraulic Fracturing by Molecular Simulations. *Phys. Chem. Chem. Phys.* **2017**, *19*, 16586-16599.

14.   Hu, Y.; Huang, L.; Zhao, S.; Liu, H.; Gubbins, K. E. Effect of Confinement in Nano-Porous Materials on the Solubility of a Supercritical Gas. *Mol. Phys.* **2016**, *114*, 3294-3306.

15.   Rakotovao, V.; Ammar, R.; Miachon, S.; Pera-Titus, M. Influence of the Mesoconfining Solid on Gas Oversolubility in Nanoliquids. *Chem. Phys. Lett.* **2010**, *485*, 299-303.

16.   Luzar, A.; Bratko, D. Gas Solubility in Hydrophobic Confinement. *J. Phys. Chem. B* **2005**, *109*, 22545-22552.

17.   Bratko, D.; Luzar, A. Attractive Surface Force in the Presence of Dissolved Gas: A Molecular Approach. *Langmuir* **2008**, *24*, 1247-1253.

18.   Borówko, M.; Patrykiejew, A.; Sokolowski, S.; Zagórski, R.; Pizio, O. Chemical Reactions at Surfaces: Application of the Reaction Ensamble Monte Carlo Method. *Czech. J. Phys.* **1998**, *48*, 371-388.

19.   Borówko , M.; Zagórski, R. Chemical Squilibria in Slitlike Pores. *J. Chem. Phys.* **2001**, *114*, 5397-5403.

20.   Turner, C. H.; Johnson, J. K.; Gubbins, K. E. Effect of Confinement on Chemical Reaction Equilibria: The Reactions $2NO \Leftrightarrow (NO)_2$ and $N_2+3H_2 \Leftrightarrow 2NH_3$ in Carbon Micropores. *J. Chem. Phys.* **2001**, *114*, 1851-1859.

21.   Turner, C. H.; Pikunic, J.; Gubbins, K. E. Influence of Chemical and Physical Surface Heterogeneity on Chemical Reaction Equilibria in Carbon Micropores. *Mol. Phys.* **2001**, *99*, 1991-2001.

22.   Turner, C. H.; Gubbins, K. E. Effects of Supercritical Clustering and Selective Confinement on Reaction Equilibrium: A Molecular Simulation Study of the Esterification Reaction. *J. Chem. Phys.* **2003**, *119*, 6057-6067.

23.   Turner, C. H.; Brennan, J. K.; Lísal, M.; Smith, W. R.; Johnson, J. K.; Gubbins, K. E. Simulation of Chemical Reaction Equilibria by the Reaction Ensemble Monte Carlo Method: A Review. *Mol. Simul.* **2008**, *34*, 119-146.

24.   Santiso, E. E.; George, A. M.; Sliwinska-Bartkowiak, M.; Nardelli, M. B.; Gubbins, K. E. Effect of Confinement on Chemical Reactions. *Adsorption* **2005**, *11*, 349-354.

25.   Turner, C. H.; Brennan, J. K.; Johnson, J. K.; Gubbins, K. E. Effect of Confinement by Porous Materials on Chemical Reaction Kinetics. *J. Chem. Phys.* **2002**, *116*, 2138-2148.

26.   Johnson, J. K.; Panagiotopoulos, A. Z.; Gubbins, K. E. Reactive Canonical Monte Carlo: A New Simulation Technique for Reacting or Associating Fluids. *Mol. Phys.* **1994**, *81*, 717-733.

27.   Smith, W. R.; Triska, B. The Reaction Ensemble Method for the Computer Simulation of Chemical and Phase Equilibria .1. Theory and Basic Examples. *J. Chem. Phys.* **1994**, *100*, 3019-3027.

28.   Peng, X.; Wang, W.; Huang, S. Monte Carlo Simulation for Chemical Reaction Equilibrium of Ammonia Synthesis in MCM-41 Pores and Pillared Clays. *Fluid Phase Equilib.* **2005**, *231*, 138-149.
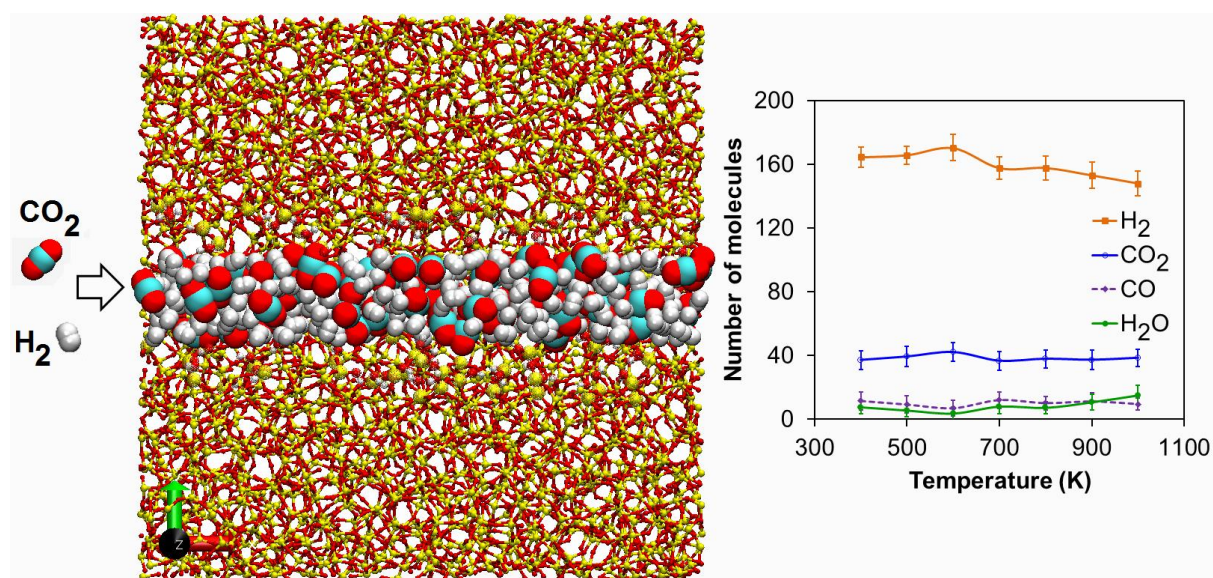
29.   Hansen, N.; Jakobtorweihen, S.; Keil, F. J. Reactive Monte Carlo and Grand-Canonical Monte Carlo Mimulations of the Propene Metathesis Reaction System. *J. Chem. Phys.* **2005**, *122*, 164705.

30.   Lísal, M.; Brennan, J. K.; Smith, W. R. Chemical Reaction Equilibrium in Nanoporous Materials: No Dimerization Reaction in Carbon Slit Nanopores. *J. Chem. Phys.* **2006**, *124*, 064712.

31.   Furmaniak, S.; Gauden, P. A.; Kowalczyk, P.; Patrykiejew, A. Monte Carlo Study of Chemical Reaction Equilibria in Pores of Activated Carbons. *RSC Adv.* **2017**, *7*, 53667-53679.

32.   Le, T.; Striolo, A.; Turner, C. H.; Cole, D. R. Confinement Effects on Carbon Dioxide Methanation: A Novel Mechanism for Abiotic Methane Formation. *Sci. Rep.* **2017**, *7:9021*.

33.   Holm, N. G. *Marine Hydrothermal Systems and the Origin of Life: Report of SCOR Working Group 91*; Kluwer, 1992.

34.   Holm, N. G.; Andersson, E. M. *The Molecular Origins of Life*; Cambride University Press: Cambridge, U.K., 1998.

35.   Moody, J. B. Serpentinization: A Review. *Lithos* **1976**, *9*, 125-138.

36.   Sleep, N. H.; Meibom, A.; Fridriksson, T.; Coleman, R. G.; Bird, D. K. H_2-Rich Fluids from Serpentinization: Geochemical and Biotic Implications. *Proceedings of the National Academy of Sciences of the United States of America* **2004**, *101*, 12818-12823.

37.   Ménez, B.; Pisapia, C.; Andreani, M.; Jamme, F.; Vanbellingen, Q. P.; Brunelle, A.; Richard, L.; Dumas, P.; Réfrégiers, M. Abiotic Synthesis of Amino Acids in the Recesses of the Oceanic Lithosphere. *Nature* **2018**, *564*, 59–63.

38.   Muchowska, K. B.; Varma, S. J.; Moran, J. Synthesis and Breakdown of Universal Metabolic Precursors Promoted by Iron. *Nature* **2019**, *569*, 104–107.

39.   Senftle, T. P.; Hong, S.; Islam, M. M.; Kylasa, S. B.; Zheng, Y.; Shin, Y. K.; Junkermeier, C.; Engel-Herbert, R.; Janik, M. J.; Aktulga, H. M., et al. The ReaxFF Reactive Force-Field: Development, Applications and Future Directions. *npj Comput. Mater.* **2016**, *2*, 15011.

40.   Han, Y.; Jiang, D.; Zhang, J.; Li, W.; Gan, Z.; Gu, J. Development, Applications and Challenges of ReaxFF Reactive Force Field in Molecular Simulations. *Front. Chem. Sci. Eng.* **2016**, *10*, 16-38.

41.   Chenoweth, K.; van Duin, A. C. T.; Goddard, W. A. ReaxFF Reactive Force Field for Molecular Dynamics Simulations of Hydrocarbon Oxidation. *J. Phys. Chem. A* **2008**, *112*, 1040-1053.

42.   Agrawalla, S.; van Duin, A. C. T. Development and Application of a ReaxFF Reactive Force Field for Hydrogen Combustion. *J. Phys. Chem. A* **2011**, *115*, 960-972.

43.   Liu, L.; Bai, C.; Sun, H.; Goddard, W. A. Mechanism and Kinetics for the Initial Steps of Pyrolysis and Combustion of 1,6-Dicyclopropane-2,4-Hexyne from ReaxFF Reactive Dynamics. *J. Phys. Chem. A* **2011**, *115*, 4941-4950.

44.   Castro-Marcano, F.; Kamat, A. M.; Russo, M. F.; van Duin, A. C. T.; Mathews, J. P. Combustion of an Illinois No. 6 Coal Char Cimulated Using an Atomistic Char Representation and the ReaxFF Reactive Force Field. *Combust. Flame* **2012**, *159*, 1272-1285.

45.   Strachan, A.; van Duin, A. C. T.; Chakraborty, D.; Dasgupta, S.; Goddard, W. A. Shock Waves in High-Energy Materials: The Initial Chemical Events in Nitramine RDX. *Phys. Rev. Lett.* **2003**, *91*, 098301.

46.   Zhang, L.; van Duin, A. C. T.; Zybin, S. V.; Goddard, W. A. Thermal Decomposition of Hydrazines from Reactive Dynamics Using the ReaxFF Reactive Force Field. *J. Phys. Chem. B* **2009**, *113*, 10770-10778.

47.   An, Q.; Liu, Y.; Zybin, S. V.; Kim, H.; Goddard, W. A. Anisotropic Shock Sensitivity of Cyclotrimethylene Trinitramine (RDX) from Compress-and-Shear Reactive Dynamics. *J. Phys. Chem. C* **2012**, *116*, 10198-10206.

48.	Ning, N.; Calvo, F.; van Duin, A. C. T.; Wales, D. J.; Vach, H. Spontaneous Self-Assembly of Silica Nanocages into Inorganic Framework Materials. *J. Phys. Chem. C* **2009**, *113*, 518-523.

49.	Bagri, A.; Mattevi, C.; Acik, M.; Chabal, Y. J.; Chhowalla, M.; Shenoy, V. B. Structural Evolution During the Reduction of Chemically Derived Graphene Oxide. *Nat Chem* **2010**, *2*, 581-587.

50.	Khalilov, U.; Pourtois, G.; van Duin, A. C. T.; Neyts, E. C. Self-Limiting Oxidation in Small-Diameter Si Nanowires. *Chem. Mater.* **2012**, *24*, 2141-2147.

51.	Iacovella, C. R.; French, W. R.; Cook, B. G.; Kent, P. R. C.; Cummings, P. T. Role of Polytetrahedral Structures in the Elongation and Rupture of Gold Nanowires. *Acs Nano* **2011**, *5*, 10065-10073.

52.	Papkov, D.; Beese, A. M.; Goponenko, A.; Zou, Y.; Naraghi, M.; Espinosa, H. D.; Saha, B.; Schatz, G. C.; Moravsky, A.; Loutfy, R., et al. Extraordinary Improvement of the Graphitic Structure of Continuous Carbon Nanofibers Templated with Double Wall Carbon Nanotubes. *Acs Nano* **2013**, *7*, 126-142.

53.	Somers, W.; Bogaerts, A.; van Duin, A. C. T.; Neyts, E. C. Interactions of Plasma Species on Nickel Catalysts: A Reactive Molecular Dynamics Study on the Influence of Temperature and Surface Structure. *Appl. Catal., B* **2014**, *154*, 1-8.

54.	Senftle, T. P.; van Duin, A. C. T.; Janik, M. J. Determining in Situ Phases of a Nanoparticle Catalyst Via Grand Canonical Monte Carlo Simulations with the ReaxFF Potential. *Catal. Commun.* **2014**, *52*, 72-77.

55.	Zhang, C.; Wen, Y.; Xue, X. Self-Enhanced Catalytic Activities of Functionalized Graphene Sheets in the Combustion of Nitromethane: Molecular Dynamic Simulations by Molecular Reactive Force Field. *ACS Appl. Mater. Interfaces* **2014**, *6*, 12235-12244.

56.	Lin, Z. Z. Graphdiyne as a Promising Substrate for Stabilizing Pt Nanoparticle Catalyst. *Carbon* **2015**, *86*, 301-309.

57.	van Duin, A. C. T.; Merinov, B. V.; Jang, S. S.; Goddard, W. A. ReaxFF Reactive Force Field for Solid Oxide Fuel Cell Systems with Application to Oxygen Ion Transport in Yttria-Stabilized Zirconia. *J. Phys. Chem. A* **2008**, *112*, 3133-3140.

58.	Bedrov, D.; Smith, G. D.; van Duin, A. C. T. Reactions of Singly-Reduced Ethylene Carbonate in Lithium Battery Electrolytes: A Molecular Dynamics Simulation Study Using the ReaxFF. *J. Phys. Chem. A* **2012**, *116*, 2978-2985.

59.	Merinov, B. V.; Mueller, J. E.; van Duin, A. C. T.; An, Q.; Goddard, W. A. ReaxFF Reactive Force-Field Modeling of the Triple-Phase Boundary in a Solid Oxide Fuel Cell. *J. Phys. Chem. Lett.* **2014**, *5*, 4039-4043.

60.	Le, T. T. B.; Striolo, A.; Cole, D. R. Structural and Dynamical Properties Predicted by Reactive Force Fields Simulations for Four Common Pure Fluids at Liquid and Gaseous Non-Reactive Conditions. *Mol. Simul.* **2018**, *44*, 826-839.

61.	Sherman, J. D. Synthetic Zeolites and Other Microporous Oxide Molecular Sieves. *Proceedings of the National Academy of Sciences of the United States of America* **1999**, *96*, 3471-3478.

62.	Primo, A.; Garcia, H. Zeolites as Catalysts in Oil Refining. *Chem. Soc. Rev.* **2014**, *43*, 7548-7561.

63.	Eslami, M.; Dekamin, M. G.; Motlagh, L.; Maleki, A. MCM-41 Mesoporous Silica: A Highly Efficient and Recoverable Catalyst for Rapid Synthesis of α-Aminonitriles and Imines. *Green Chem. Lett. Rev.* **2018**, *11*, 36-46.

64.	Thampi, K. R.; Kiwi, J.; Grätzel, M. Methanation and Photo-Methanation of Carbon Dioxide at Room Temperature and Atmospheric Pressure. *Nature* **1987**, *327*, 506-508.

65.	Solymosi, F.; Erdöhelyi, A.; Kocsis, M. Methanation of CO_2 on Supported Ru Catalysts. *J. Chem. Soc., Faraday Trans. 1* **1981**, *77*, 1003-1012.

66.   Krämer, M.; Stöwe, K.; Duisberg, M.; Müller, F.; Reiser, M.; Sticher, S.; Maier, W. F. The Impact of Dopants on the Activity and Selectivity of a Ni-Based Methanation Catalyst. *Appl. Catal., A* **2009**, *369*, 42-52.

67.   Du, G. A.; Lim, S.; Yang, Y.; Wang, C.; Pfefferle, L.; Haller, G. L. Methanation of Carbon Dioxide on Ni-Incorporated MCM-41 Catalysts: The Influence of Catalyst Pretreatment and Study of Steady-State Reaction. *J. Catal.* **2007**, *249*, 370-379.

68.   Martin, N. M.; Velin, P.; Skoglundh, M.; Bauer, M.; Carlsson, P. A. Catalytic Hydrogenation of CO_2 to Methane over Supported Pd, Rh and Ni Catalysts. *Catal. Sci. Technol.* **2017**, *7*, 1086-1094.

69.   Le, T. A.; Kim, M. S.; Lee, S. H.; Park, E. D. CO and CO_2 Methanation over Supported Cobalt Catalysts. *Top. Catal.* **2017**, *60*, 714-720.

70.   Abe, T.; Tanizawa, M.; Watanabe, K.; Taguchi, A. CO_2 Methanation Property of Ru Nanoparticle-Loaded TiO_2 Prepared by a Polygonal Barrel-Sputtering Method. *Energy Environ. Sci.* **2009**, *2*, 315-321.

71.   Zhou, L.; Wang, Q.; Ma, L.; Chen, J.; Ma, J.; Zi, Z. CeO_2 Promoted Mesoporous Ni/γ-Al_2O_3 Catalyst and Its Reaction Conditions for CO_2 Methanation. *Catal. Lett.* **2015**, *145*, 612-619.

72.   Jwa, E.; Lee, S. B.; Lee, H. W.; Mok, Y. S. Plasma-Assisted Catalytic Methanation of CO and CO_2 over Ni-Zeolite Catalysts. *Fuel Process. Technol.* **2013**, *108*, 89-93.

73.   Kim, H. Y.; Lee, H. M.; Park, J. N. Bifunctional Mechanism of CO_2 Methanation on Pd-MgO/SiO_2 Catalyst: Independent Roles of MgO and Pd on CO_2 Methanation. *J. Phys. Chem. C* **2010**, *114*, 7128-7131.

74.   Mortier, W. J.; Ghosh, S. K.; Shankar, S. Electronegativity Equalization Method for the Calculation of Atomic Charges in Molecules. *J. Am. Chem. Soc.* **1986**, *108*, 4315-4320.

75.   Newsome, D. A.; Sengupta, D.; Foroutan, H.; Russo, M. F.; van Duin, A. C. T. Oxidation of Silicon Carbide by O_2 and H_2O: A ReaxFF Reactive Molecular Dynamics Study, Part I. *J. Phys. Chem. C* **2012**, *116*, 16111-16121.

76.   van Duin, A. C. T.; Dasgupta, S.; Lorant, F.; Goddard, W. A. ReaxFF: A Reactive Forcefield for Hydrocarbons. *J. Phys. Chem. A* **2001**, *105*, 9396-9409.

77.   van Duin, A. C. T.; Strachan, A.; Stewman, S.; Zhang, Q.; Xu, X.; Goddard, W. A. ReaxFF$_{SiO}$ Reactive Force Field for Silicon and Silicon Oxide Systems. *J. Phys. Chem. A* **2003**, *107*, 3803-3811.

78.   Fogarty, J. C.; Aktulga, H. M.; Grama, A. Y.; van Duin, A. C. T.; Pandit, S. A. A Reactive Molecular Dynamics Simulation of the Silica-Water Interface. *J. Chem. Phys.* **2010**, *132*, 174704.

79.   Buehler, M. J.; van Duin, A. C. T.; Goddard, W. A. Multiparadigm Modeling of Dynamical Crack Propagation in Silicon Using a Reactive Force Field. *Phys. Rev. Lett.* **2006**, *96*, 095505.

80.   Chenoweth, K.; Cheung, S.; van Duin, A. C. T.; Goddard, W. A.; Kober, E. M. Simulations on the Thermal Decomposition of a Poly(dimethylsiloxane) Polymer Using the ReaxFF Reactive Force Field. *J. Am. Chem. Soc.* **2005**, *127*, 7192-7202.

81.   Aktulga, H. M.; Fogarty, J. C.; Pandit, S. A.; Grama, A. Y. Parallel Reactive Molecular Dynamics: Numerical Methods and Algorithmic Techniques. *Parallel Comput.* **2012**, *38*, 245-259.

82.   Plimpton, S. Fast Parallel Algorithms for Short-Range Molecular Dynamics. *J. Comput. Phys.* **1995**, *117*, 1-19.

83.   Le, T. T. B.; Striolo, A.; Gautam, S. S.; Cole, D. R. Propane–Water Mixtures Confined within Cylindrical Silica Nanopores: Structural and Dynamical Properties Probed by Molecular Dynamics. *Langmuir* **2017**, *33*, 11310-11320.

84.   D'Souza, A. S.; Pantano, C. G. Mechanisms for Silanol Formation on Amorphous Silica Fracture Surfaces. *J. Am. Ceram. Soc.* **1999**, *82*, 1289-1293.

85.   Gao, J.; Wang, Y.; Ping, Y.; Hu, D.; Xu, G.; Gu, F.; Su, F. A Thermodynamic Analysis of Methanation Reactions of Carbon Oxides for the Production of Synthetic Natural Gas. *RSC Adv.* **2012**, *2*, 2358-2368.

86.   Jablonka, K. M.; Ongari, D.; Smit, B. Applicability of Tail Corrections in the Molecular Simulations of Porous Materials. *J. Chem. Theory Comput.* **2019**.

87.   Liu, L.; Liu, Y.; Zybin, S. V.; Sun, H.; Goddard, W. A. ReaxFF-Lg: Correction of the ReaxFF Reactive Force Field for London Dispersion, with Applications to the Equations of State for Energetic Materials. *J. Phys. Chem. A* **2011**, *115*, 11016-11022.

88.   Chaban, V. V.; Fileti, E. E.; Prezhdo, O. V. Buckybomb: Reactive Molecular Dynamics Simulation. *J. Phys. Chem. Lett.* **2015**, *6*, 913-917.

89.   Pai, S. J.; Yeo, B. C.; Han, S. S. Development of the ReaxFF(CBN) Reactive Force Field for the Improved Design of Liquid CBN Hydrogen Storage Materials. *Phys. Chem. Chem. Phys.* **2016**, *18*, 1818-1827.

90.   Jacquemin, M.; Beuls, A.; Ruiz, P. Catalytic Production of Methane from CO_2 and H_2 at Low Temperature: Insight on the Reaction Mechanism. *Catal. Today* **2010**, *157*, 462-466.

91.   Park, J. N.; McFarland, E. W. A Highly Dispersed Pd-Mg/SiO_2 Catalyst Active for Methanation of CO_2. *J. Catal.* **2011**, *266*, 92-97.

92.   Smith, J. M.; Van Ness, H. C.; Abbott, M. M. *Introduction to Chemical Engineering Thermodynamics*; McGraw-Hill: Boston, 2005.

93.   Koretsky, M. D. *Engineering and Chemical Thermodynamics*; John Wiley & Sons, Inc.: New York, 2013.

94.   Bai, C.; Liu, L. C.; Sun, H. Molecular Dynamics Simulations of Methanol to Olefin Reactions in HZSM-5 Zeolite Using a ReaxFF Force Field. *J. Phys. Chem. C* **2012**, *116*, 7029-7039.

95.   Zhang, Z.; Yan, K.; Zhang, J. ReaxFF Molecular Dynamics Simulations of Non-Catalytic Pyrolysis of Triglyceride at High Temperatures. *RSC Adv.* **2013**, *3*, 6401-6407.

96.   Liu, I.; Cant, N. W.; Bromly, J. H.; Barnes, F. J.; Nelson, P. F.; Haynes, B. S. Formate Species in the Low-Temperature Oxidation of Dimethyl Ether. *Chemosphere* **2001**, *42*, 583-589.

97.   Taatjes, C. A.; Meloni, G.; Selby, T. M.; Trevitt, A. J.; Osborn, D. L.; Percival, C. J.; Shallcross, D. E. Direct Observation of the Gas-Phase Criegee Intermediate (CH_2OO). *J. Am. Chem. Soc.* **2008**, *130*, 11883-11885.

98.   He, Z.; Li, X. B.; Liu, L. M.; Zhu, W. The Intrinsic Mechanism of Methane Oxidation under Explosion Condition: A Combined ReaxFF and DFT Study. *Fuel* **2014**, *124*, 85-90.

99.   Griscom, D. L. Defect Structure of Glasses: Some Outstanding Questions in Regard to Vitreous Silica. *J. Non-Cryst. Solids* **1985**, *73*, 51-77.

100.   Pan, Y. X.; Liu, C. J.; Mei, D.; Ge, Q. Effects of Hydration and Oxygen Vacancy on CO_2 Adsorption and Activation on β-Ga_2O_3(100). *Langmuir* **2010**, *26*, 5551-5558.

101.   Huygh, S.; Bogaerts, A.; Neyts, E. C. How Oxygen Vacancies Activate CO_2 Dissociation on TiO_2 Anatase (001). *J. Phys. Chem. C* **2016**, *120*, 21659-21669.

102.   Jiang, Q.; Chen, Z.; Tong, J.; Yang, M.; Jiang, Z.; Li, C. Direct Thermolysis of CO_2 into CO and O_2. *Chem. Commun.* **2017**, *53*, 1188-1191.

103.   Weismiller, M. R.; Junkermeier, C. E.; Russo, M. F.; Salazar, M. R.; Bedrov, D.; van Duin, A. C. T. ReaxFF Molecular Dynamics Simulations of Intermediate Species in Dicyanamide Anion and Nitric Acid Hypergolic Combustion. *Model Simul Mater Sc* **2015**, *23*, 074007.

104.   Page, A. J.; Moghtaderi, B. Molecular Dynamics Simulation of the Low-Temperature Partial Oxidation of CH_4. *J. Phys. Chem. A* **2009**, *113*, 1539-1547.

105.   Cole, D.; Striolo, A. In *Deep Carbon: Past to Present*; Orcutt, B.; Daniel, I.; Dasgupta, R., Eds.; Cambridge University Press: Cambridge, U. K., 2019.

TOC Graphic